Enhanced Spin Interactions in Digital Magnetic Heterostructures

S. A. Crooker, D. A. Tulchinsky, J. Levy, and D. D. Awschalom
Department of Physics, University of California, Santa Barbara, California 93106

R. Garcia and N. Samarth
Department of Physics, The Pennsylvania State University, University Park, Pennsylvania 16802
(Received 5 December 1994)

A new heterostructure is developed in which fractional monolayers of magnetic ions are introduced "digitally" within a semiconductor quantum well. Rearranging moments within two-dimensional (2D) planes provides additional control over their interactions, yielding tunable two-level electronic systems in which spin splittings are significantly larger than inhomogeneous linewidths in modest magnetic fields. Femtosecond-resolved electronic and magnetic spectroscopies reveal spin-flip scattering dependent only on the Zeeman energy but not the local magnetic environment, and long-lived dynamic magnetizations.

PACS numbers: 73.20.Dx, 75.50.Rr, 78.20.Ls, 78.47.+p

Experimental studies of electronic spin scattering are important for gaining insight into a variety of physical phenomena in condensed matter systems that involve confined and interfacial geometries such as III-V semiconductor quantum wells [1], metallic multilayers [2], granular magnetic materials [3], and magnetic semiconductor quantum structures [4]. The latter class of systems is particularly appealing as it provides a unique nexus between low-dimensional magnetism and semiconductor quantum confinement, allowing one to systematically interrogate the connection between electronic spin scattering and factors such as interfacial disorder, magnetic environment, and the degree of quantum confinement. To this end, we have developed new "digital magnetic heterostructures" (DMH) in which interactions between localized magnetic spins and their overlap with quantum-confined electronic states are tailored through a controlled digital distribution of two-dimensional (2D) magnetic layers. This class of quantum structure provides a widely tunable two-level electronic spin system with qualitatively different dynamical interactions than those seen in traditional diluted magnetic semiconductor (DMS) alloys.

We present a comprehensive investigation of exciton spin-scattering and dynamic magnetization processes in DMH using both steady-state and time-resolved magneto-optical spectroscopies. Polarization-resolved luminescence measurements reveal spin-flip scattering between Zeeman-split levels that is strongly dependent on the energy splitting but *not* the local magnetic environment. These spin-engineered structures generate a giant "quantum-confined" Faraday effect with optical rotations $\sim 10^7$ deg/cm T. Following the picosecond electronic scattering process, Faraday rotation shows an induced magnetization with a remarkably slow temperature-dependent spin-lattice relaxation persisting to microsecond time scales. In contrast to alloyed magnetic semiconductors, rearranging the fixed number of moments within a comb of planes in otherwise identical quantum wells changes the number of nearest-neighbor interactions, enabling spin-dependent effects unlike those seen in three-dimensional alloys.

A series of six samples are formed using single 120 Å $Zn_{0.80}Cd_{0.20}Se$ quantum wells fabricated by molecular beam epitaxy on a (100) GaAs substrate with a 7000 Å ZnSe buffer and a 1000 Å ZnSe cap layer. During the growth of the 39-monolayer (ML) heterostructure, 3 ML of the wide band-gap magnetic semiconductor MnSe are substituted systematically in varied distributions [Fig. 1(a)]. Two samples consist of a single 3-ML MnSe barrier in the center of the nonmagnetic well (termed 1×3 ML) and a nonmagnetic control. The remaining structures incorporate 2D distributions of spins including one with three equispaced MnSe monolayers (3×1 ML), continuing through $6 \times \frac{1}{2}$, $12 \times \frac{1}{4}$, and $24 \times \frac{1}{8}$ ML. The average Mn composition in each sample is therefore maintained at ~8%. All layer thicknesses are accurately determined to within a few percent using *in situ* reflection high-energy electron diffraction techniques. This scheme allows control of the magnetic disorder along the growth direction, the in-plane magnetic spin density, the shape of the band electron wave functions, and the spatial overlap of these wave functions with the localized Mn spins [5]. Figure 1(a) shows the envelope functions of confined conduction electron states calculated from a simple single-electron solution to the Schrödinger equation for three geometries using known band structure parameters [6].

Low-temperature static photoluminescence (PL) and absorption studies are performed using the Faraday configuration in $B \leq 8$ T. All samples reveal sharp heavy-hole (hh) exciton peaks with small Stokes shifts (~3 meV) whose FWHM (~6 meV) are attributed to inhomogeneous broadening caused by nonmagnetic alloy and well width fluctuations. An applied magnetic field splits the exciton into lower (spin-down, $S_z = +1$) and higher energy

0031-9007/95/75(3)/505(4)$06.00

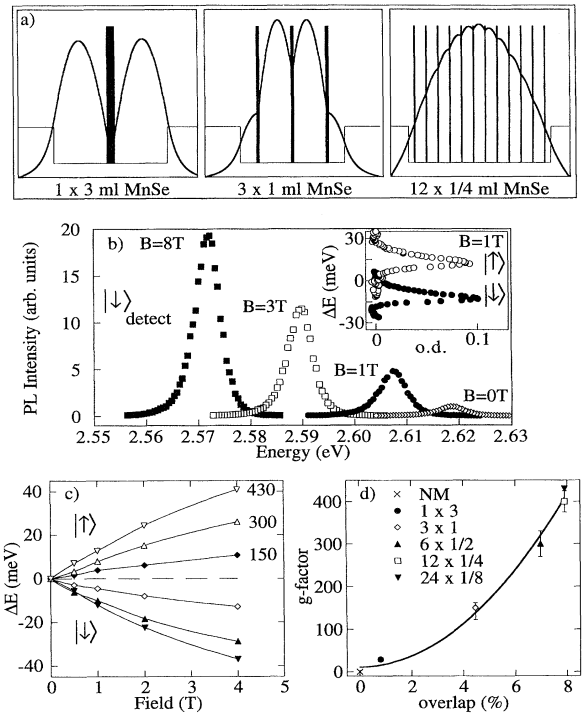

FIG. 1. (a) Schematic diagram of the conduction band energy profiles and electron wave functions. (b) PL from the spin-down state of the $24 \times \frac{1}{8}$ ML DMH at 5 K in various fields using 750 μW. Inset: Optical density of the spin-split exciton absorption peaks. (c) Zeeman splittings and g factors of the exciton absorption peaks as a function of the magnetic field at 5 K. Lines are guides to the eye. (d) Low field g factors vs the calculated wave-function overlap with the MnSe barriers.

(spin-up, $S_z = -1$) states due to the sp-d exchange interaction [7] resulting from the overlap of the electron and hole wave functions and the distributed Mn spins. The polarization-resolved magneto-PL from recombining spin-down excitons is shown in Fig. 1(b). The PL linewidths and corresponding absorption oscillator strengths are independent of applied fields and are nearly the same as from the control structure, indicating little change in the electronic confinement [8]. The spin-split absorption spectra depicted in the inset of Fig. 1(b) illustrate how DMH can provide prototypes of field-tunable two-level spin systems, in which the spin splittings are significantly larger than the inhomogeneous absorption linewidths even in modest magnetic fields (1 T). Successive division of the magnetic layers produces two clear results: increased penetration of the wave function into the Mn barriers which increases the g factor [Fig. 1(c)] and a reduction of the wave-function curvature causing the luminescence peaks to shift to lower energy. Both effects reflect significant changes in the Mn distribution. More subtle effects relate directly to changes in the local magnetic environment. Figure 1(d) shows a superlinear dependence of the g factor as a function of the electronic overlap with the magnetic regions, and is likely due to an increase in the number of uncompensated paramagnetic spins.

Insights into electronic spin scattering processes are obtained through studies of the PL polarization, quantum efficiency, and exciton lifetime. Strong polarization $P = (I\downarrow - I\uparrow)/(I\downarrow + I\uparrow)$ of the PL as a function of the magnetic field is caused by preferential spin scattering to the energetically favorable spin-down state [Fig. 2(a)]. Figure 2(b) shows that the polarizations scale with the Zeeman energy splitting ΔE and are insensitive to their relative magnetizations $\langle S_z \rangle$. For a two-level system in thermal equilibrium, the relative population of the spin-split energy states yields a polarization given by $P(\Delta E) = \tanh(\Delta E/2k_BT)$. The exciton polarization of the 2D samples fits this functional form [Fig. 2(b)] with an effective temperature $T = 35$ K ~ 3 meV/k_B. At $T = 5$ K, $P(\Delta E)$ implies that the spin-polarized carrier populations do not reach thermodynamic equilibrium. The origin of the emitted polarization is confirmed by the relative intensities and lifetimes of the spin-up and spin-down PL [Figs. 2(c) and 2(d)]: Recombining spin-down excitons show a large increase in PL intensity accompanied by an

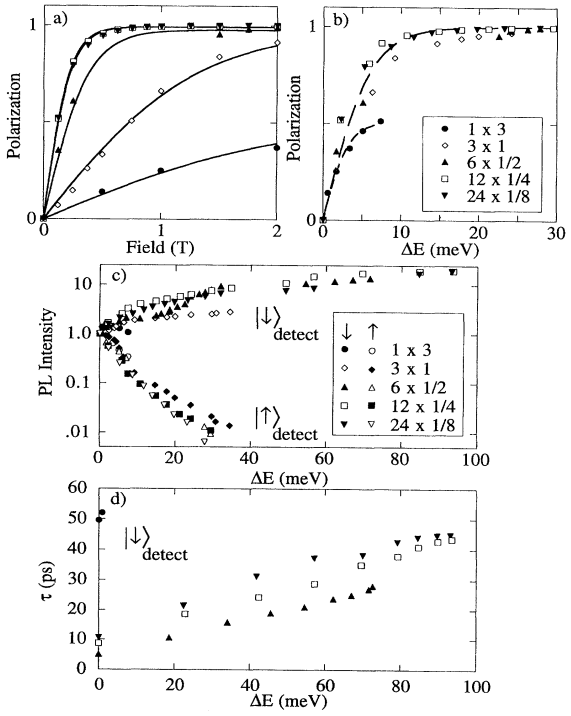

FIG. 2. (a) Field dependence of the static exciton PL polarization at 5 K from the DMH indicated in Fig. 1(b). (b) PL polarization vs Zeeman splitting at 5 K. (c) Peak PL intensities (normalized at zero field) at various Zeeman splittings at 5 K. (d) PL lifetimes vs Zeeman splitting at 5 K using a streak camera from the DMH indicated in Fig. 1(b).

increase in carrier lifetime, while spin-up excitons exhibit the opposite behavior. Having little effect on the electronic confinement, the applied field increases radiative recombination from the lower energy spin-down state relative to the defect-related nonradiative relaxation channels. In contrast, the behavior of the 1×3 ML structure is closer to that seen in DMS and consistent with the evidence of bulklike behavior in 3 ML of MnSe [9,10].

A direct picture of ultrafast spin dynamics is obtained using femtosecond-resolved up-conversion PL measurements allowing one to directly observe polarized luminescence from photoexcited excitons as they undergo spin scattering [4,10]. Figures 3(a) and 3(b) show the time-resolved polarization of the emitted PL from the $24 \times \frac{1}{8}$ ML structure when spin-down (spin-up) exciton populations are created with 120 fs pulses of right (left) circularly polarized light. In zero field, the polarization decays symmetrically to zero yielding a spin-scattering time $\tau_{sf} \sim 6$ ps. The removal of the spin degeneracy by a magnetic field results in the majority of spin-up excitons scattering into the lower energy spin-down state. As seen in Fig. 3(c), the time evolution of the two spin populations in the 2D DMH structures is determined *solely* by the Zeeman splitting, where the spin relaxation for each magnetic sample is measured at $\Delta E = 3$ meV. A characteristic spin-scattering time $\tau_{sf}(\Delta E)$ is obtained from the initial slope of the time-resolved data [Fig. 3(d)]. The results indicate that τ_{sf} for spin reversal from spin up to spin down decreases with increasing ΔE in all the 2D DMH structures, while τ_{sf} in the 1×3 ML system is seen to be only weakly dependent on applied field. The asymmetric dynamics of oriented excitons in the 1×3 ML sample [Fig. 3(c)] resemble those seen in comparable DMS heterostructures [10,11] where the spin populations fail to reach equilibrium within their lifetime.

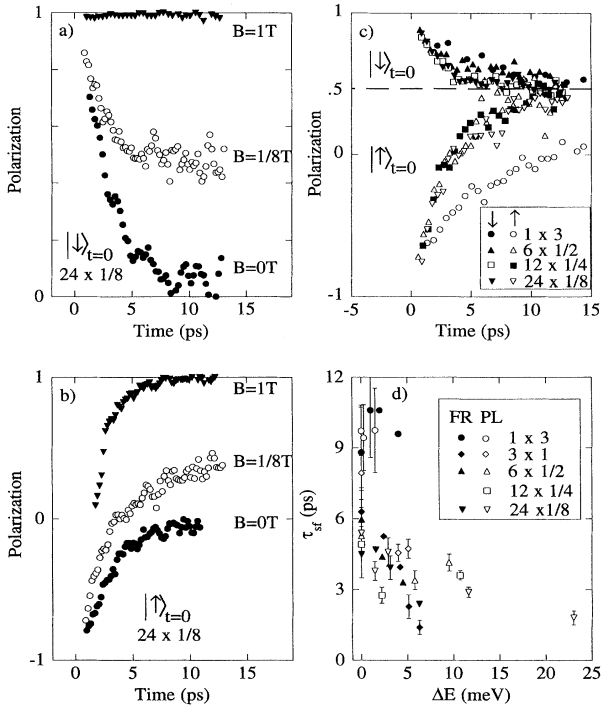

FIG. 3. (a), (b) Time-resolved polarization at $T = 4.6$ K excited 25 meV above the zero-field PL peak in magnetic fields from excitons initially oriented (a) spin down and (b) spin up. (c) Time-resolved polarization at $\Delta E = 3$ meV Zeeman splitting ($\Delta E = 5$ meV for the 1×3 ML sample) from excitons injected spin up and spin down. (d) The spin-flip times at different energy splittings. Open (closed) symbols are derived from the time-resolved polarization (Faraday rotation).

Studies of both the static and time-resolved Faraday rotation (FR) reveal not only the electronic dynamics of spin-polarized excitons in the quantum well, but also the evolution of perturbations to the Mn sublattice after the excitons have recombined. Static FR measurements clearly reveal both the $n = 1$ and $n = 2$ hh-exciton resonances [12]. The combination of narrow absorption lines and large g factors result in enormous optical rotations—a single 120 Å DMH in $B < 50$ mT elicits a rotation of $\theta_F = 22$ deg/T, corresponding to a Verdet constant of $\sim 1.8 \times 10^7$ deg/cm T. In time-resolved measurements [4,11], a femotosecond optical pump pulse (~ 50 pJ) tuned to the zero-field resonance photoexcites spin-polarized excitons and generates changes in the magnetization of the system, measured through the FR imparted to a weaker

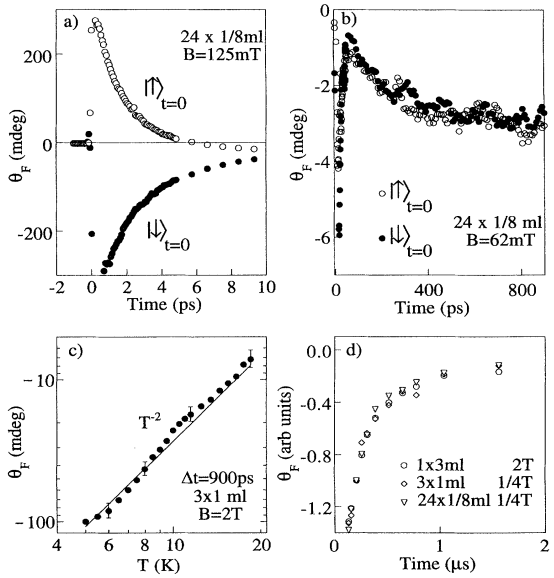

FIG. 4. (a) Time-resolved Faraday rotation (TRFR) in the $24 \times \frac{1}{8}$ ML DMH at 5 K, revealing exciton recombination and preferential spin-flip scattering to the spin-down state. (b) *Orientation-independent* decrease in the TRFR in low fields long after carrier recombination. (c) Temperature dependence of the TRFR at $\Delta t = 900$ ps. (d) Persistent TRFR in DMH (each normalized to its 200 ns value).

time-delayed probe pulse. Figure 4(a) shows the time-resolved FR in the ultrafast regime where contributions sensitive to the relative populations of two Zeeman-split exciton states dominate. The initial decay of θ_F matches the rapid spin scattering and carrier recombination seen in the time-resolved PL data, and is only weakly dependent on temperature. Note that when pumping the spin-up state, a majority of these carriers have spin flipped by ~6 ps, resulting in the *negative* value of θ_F. A spin-scattering time is extracted from the short-time FR data and is also shown in Fig. 3(d).

The dynamic FR on time scales longer than the carrier lifetime reflects changes in the magnetization of the perturbed Mn spins. In low magnetic fields, the FR develops a local maximum which is seen to arise from the superposition of the decay of the few remaining excitons with the onset of the magnetic response. The magnetic contribution to θ_F [Fig. 4(b)] rises initially from zero to a maximum near 800 ps, then decays over a time scale ~1 μs [see Fig. 4(d)]. In contrast to earlier studies in DMS [4,11] both the sign and the magnitude of the long-lived pump-induced magnetization are *independent* of the initial carrier orientation for all the DMH structures. At higher magnetic fields and temperatures, the onset and decay times decrease rapidly, the former eventually becoming masked by the longer-lived excitonic contributions. The magnitude of the long-lived ($\Delta t = 900$ ps) magnetic signature displays a T^{-2} dependence when cooled in constant field [Fig. 4(c)]. Similar measurements taken at constant Zeeman splitting ($\sim B/T$ for small B) reveal a T^{-1} temperature dependence. These dependencies are in agreement with the expectation that $\theta_F \propto \Delta M \propto B\Delta T/T^2$, implying that carrier induced heating of the magnetic subsystem is responsible. Neither result is consistent with simple lattice heating, where T^3 contributions due to the specific heat predict temperature dependences of T^{-5} and T^{-4}, respectively. As shown in Fig. 4(d), the long-lived signal persists to microsecond times in all of the samples.

Both the time-resolved PL and FR show that the electronic and magnetic behaviors of DMH structures are affected unexpectedly by the planar arrangement of the magnetic spins within the quantum well. Unlike bulk materials, neutron diffraction studies of ZnSe/MnSe multilayers indicate that strain-induced crystal fields break the symmetry between nearest-neighbor spins and cause the moments to lie in the plane [9]. An excess density of uncompensated spins in the dilute 2D DMH structures should yield a larger g factor than for DMS due to a reduction of nearest neighbors in a planar environment from 12 to 4. However, the large g factor observed in the 3×1 ML sample suggests that clusters of magnetic spins oriented in the growth plane still contribute to the sp-d exchange [13]. Orientation-dependent magnetic signatures, generated by the direct transfer of exciton angular momentum to the magnetic sublattice observed in earlier DMS studies [4,11] do not appear in DMH. These long-lived magnetic dynamics are surprisingly insensitive to the distribution of magnetic spins and applied field [Fig. 4(d)], suggesting phonon mediated relaxation processes [11,14].

In summary, changing the texture between magnetic and nonmagnetic layers in DMH generates completely different electronic and magnetic spin interactions than seen in DMS. Electronic spin scattering appears to be decoupled from direct spin-exchange interactions with the local magnetic environment. These engineered planar structures restrict the dimensionality of magnetic interactions thereby increasing their overlap with electronic states, and exhibit behavior akin to models of a giant magnetoresistance.

We thank J. J. Baumberg for helpful comments. This work was supported by Grants No. NSF DMR 92-07567 and No. STC DMR 91-20007, No. ONR N00014-94-1-0297 and -0225, and No. AFOSR F49620-93-1-0446.

[1] S. Bar-Ad and I. Bar-Joseph, Phys. Rev. Lett. **66**, 2491 (1991); T. Uenoyma and L. J. Sham, *ibid.* **64**, 3070 (1990); G. Bastard and L. L. Chang, Phys. Rev. B **41**, 7899 (1990).
[2] Q. Yang *et al.,* Phys. Rev. Lett. **72**, 3274 (1994).
[3] A. E. Berkowitz *et al.,* Phys. Rev. Lett. **68**, 3745 (1992); J. Q. Xiao, J. S. Lang, and C. L. Chien, *ibid.* **68**, 3749 (1992).
[4] J. F. Smyth *et al.,* Phys. Rev. Lett. **71**, 601 (1993); J. J. Baumberg *et al., ibid.* **72**, 717 (1994.
[5] This is the magnetic analog of the "digital alloy" concept first introduced in purely semiconductor quantum structures to generate confining potentials of desired shapes. See R. C. Miller *et al.,* Phys. Rev. B **29**, 3740 (1984).
[6] R. B. Bylsma *et al.,* Phys. Rev. B **33**, 8207 (1986); N. Samarth *et al.,* Appl. Phys. Lett. **56**, 1163 (1990).
[7] *Diluted Magnetic Semiconductors,* edited by J. K. Furdyna and J. Kossut (Academic Press, San Diego, 1988), Vol. 25.
[8] While details concerning the incorporation of fractional MnSe layers on ZnCdSe surfaces are unknown, the results suggest a relatively uniform distribution of Mn on scales larger than the exciton Bohr radius. See P. M. Petroff, A. C. Gossard, and W. Wiegmann, Appl. Phys. Lett. **45**, 620 (1984).
[9] N. Samarth *et al.,* Phys. Rev. B **44**, 4701 (1991).
[10] D. A. Tulchinsky *et al.,* Phys. Rev. B **50**, 10 851 (1994).
[11] J. J. Baumberg *et al.,* Phys. Rev. B **50**, 7689 (1994).
[12] S. A. Crooker, D. D. Awschalom, and N. Samarth (to be published).
[13] W. J. Ossau and B. Kuhn-Heinrich, Physica (Amsterdam) **184B**, 422 (1993).
[14] E. A. Harris and K. S. Yngvesson, J. Phys. C **1**, 990 (1968).